

Electron Transport Properties of Ternary alloys Gallium Indium Phosphide

C. Sayah^a, B. Bouazza^b, A. Guen-Bouazza^b And N. E. Chabane-Sari^b

^aLaboratoire de Structures Intelligentes, Ctr Univ Ain Temouchent, Institut des Sciences et de la Technologie, BP 284- 46000AinTemouchent /Algerie

^bUnité de recherche des matériaux et des énergies renouvelables, Faculté des sciences de l'ingénieur, Université Abou-BekrBelkaid de Tlemcen. BP 230, Tlemcen 13000, Algérie.

Corresponding author: email: (a) chou28dz@gmail.com, (b) bouaguen@yahoo.fr

Received date: November 24, 2016; revised date: May 20, 2017; accepted date: May 23, 2017

Abstract

This paper deals with the development and application of Monte Carlo simulations to study electron transport in bulk $Ga_{1-x}In_xP$ in the zinc blende crystal structure. The simulation model includes three sets of non-parabolic conduction band valleys which can be occupied by electrons during high field transport. The effects on electron transport of impurities and the relevant phonon scattering mechanisms have been considered. The dependence of the transport properties on the material parameters is discussed and also with regard to the temperature, donor concentration. We have introduced and examined the effects of alloy concentration of bulk $Ga_{1-x}In_xP$, and how this affects the transport properties, especially the average drift velocity, predicted by our Monte-Carlo simulation programs.

Keywords: Monte Carlo method, semiconductor materials, phonon scattering mechanisms, alloys scattering mechanisms, $Ga_{1-x}In_xP$

1. Introduction

In the development field of new materials, the compound semiconductors continue being an area of great interest and rapid expansion [1-2]. The advantage of alloying is that the alloy properties, such as band gap, can be tuned by varying the alloy composition to meet the specific requirements of modern device applications [3-4]. Indium gallium phosphide (InGaP) is a ternary semiconductor composed of InP and GaP. **Fig. 1** illustrates the band gap energy transition from InP to GaP, where the black solid line shows direct band gap transitions, and the black dashed line describes the indirect band gap transition. Band gap energy and lattice constant values are between the corresponding values of the binary alloys from which it is formed. It is an important alloy for the development of lighting emitting devices, photovoltaic systems, high-power and high-frequency electronics, due to the capacity to control the band gap, which varies according to the indium concentration in a range of energies from 2.26 eV to 1.27 eV [1-5]. Especially the $Ga_{0.5}In_{0.5}P$ is an alloy of significant importance because it can be lattice matched to GaAs. L'InGaP is used mainly in high electron mobility transistor (HEMT) and heterojunction bipolar transistors (HBT) and it has attracted many attentions in high speed and power applications due to the superior transport properties [6], it is also used for the fabrication of high efficiency solar cell

used for space applications and, in combination with Aluminium (AlInGaP alloy) to make high brightness laser emission diode with orange-red, orange, yellow, and green colors. $Ga_{0.5}In_{0.5}P$ is used as the high energy junction on double and triple junction photovoltaic cells grown on GaAs [7]. Growth of GaInP by epitaxy can be complicated by the tendency of GaInP to grow as an ordered material, rather than a truly random alloy [8]. The variation of composition for $In_xGa_{1-x}P$ has a marked influence on the splitting of reduction of its energy gap as well as on the splitting of its valence and conduction bands [9].

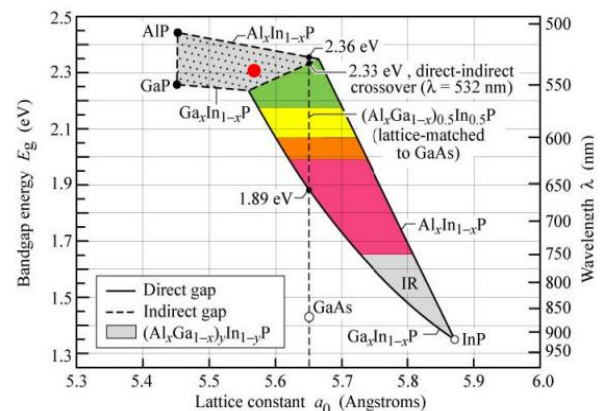


Fig.1. Band gap energy and corresponding wavelength versus lattice constant of $Ga_{1-x}In_xP$ at 300K [19].

For the purposes of this analysis of the steady-state electron transport within InP, GaP and GaIn_xP. We employ a single semi-classical three-valley Monte Carlo simulation approach. The scattering mechanisms considered are: ionized impurity, polar optical phonon, piezoelectric, acoustic deformation potential and Intervalley scattering. To simulate electron transport in alloys it is necessary to include alloy scattering in the transport model. The alloy scattering is in addition to the scattering mechanisms present in elements and compounds which do not have this chemical disorder. In this model the alloy disorder is considered to be produced by a set of short range scatterers [10-11]. If the A and B atoms are arranged randomly without any correlation the alloy scattering rate, W_{all} is [10-11-12-13]:

$$W_{all}(\varepsilon) = \frac{3 \cdot \pi^3}{8 \cdot \hbar} \cdot V_0 U_{all}^2 \cdot x(1-x) \cdot N(\varepsilon)$$

Where V_0 is the volume of the primitive cell, U_{all} is random alloy potential, x is Al mole fraction and $N(\varepsilon)$ is the density of states. Different interpretations for the choice of the random alloy potential have been given in the past. Littlejohn et al. [14] have used the conduction band offset to represent the random scattering potential, whilst another is to use the differences in their electron affinities [10-11]. Other workers have fitted values to experimental transport data to obtain a value of 0.42e V [15-16]. Chin et al. [17] have determined the random potential from band gap bowing parameters and applying Phillips' theory of electro negativity differences [18]. Because of the large number of alloys available, each with a continuous range of compositions, the band structure and related parameters are generally not available from experiment. Interpolation between the end point binary materials is normally used to obtain band structure and scattering parameters [10-11-15-20-21].

The values of most interest are the conduction band valley separations and their effective masses. We have used linear interpolation for these parameters. Indium gallium phosphide (InGaP) is a semiconductor composed of indium, gallium and phosphorus. Alloy scattering for GaIn_xP are simulated using alloy potentials expressed as and where:

$$\Delta U^2 = x(1-x) \left| \varepsilon_{gInP} - \varepsilon_{gGaP} \right|^2$$

$\varepsilon_{gInP}, \varepsilon_{gGaP}$ are the band gaps for InP and GaP, respectively. For our simulations, the crystal temperature is set to 300 K and the doping concentration is set to 10^{17}cm^{-3} for all cases. The influence of holes in the valence band is completely neglected. The conduction band is approximated by the Γ valley centered at (0,0,0), four equivalent L valleys along (1,1,1) and three equivalent X valleys along (1,0,0).

2. Material parameter

For a ternary alloy $A_x B_{1-x} N$ the dependence of a parameter y on the mole fraction x is usually approximated as:

$$y_{A_x B_{1-x} N} = x \cdot y_{AN} + (1-x) y_{BN} - b \cdot x(1-x)$$

Where the deviation from linear behavior is considered using the bowing factor b . The band gap is one of the most important semiconductor parameters. The Varshni equation has been used until now to describe the band gap dependence on the temperature for almost all the III-V semiconductors [22]. The band gap of InP, GaP [23] and In_{0.5}Ga_{0.5}P [24] can be given by:

$$\begin{aligned} E_g(T) &= 1,421 - 4,9 \cdot 10^{-4} \frac{T^2}{T + 327} \\ E_g(T) &= 2,34 - 6,2 \cdot 10^{-4} \frac{T^2}{T + 460} \\ E_g(T) &= 1,937 - 6,12 \cdot 10^{-4} \frac{T^2}{T + 204} \end{aligned}$$

The band gap is then calculated depending on the material composition. This is important to assure consistency between the values for alloy materials at $x=0$ and $x=1$ and the values for the respective basic materials. In **Fig. 2** the material composition dependence of the Γ , L, and X band gaps in GaIn_xP at 300 K is shown. Energy separations between Γ , L and X conduction band minima and top of the valence band:

At 10 K [25]

$$\begin{aligned} E_a^\Gamma &= 1,418 + 0,77x + 0,648x^2 \\ E_g^X &= 2,369 - 0,152x + 0,147x^2 \end{aligned}$$

At 77 K [26]

$$\begin{aligned} E_a^\Gamma &= 1,405 + 0,702x + 0,764x^2 \\ E_g^X &= 2,248 + 0,072x \end{aligned}$$

At 300 K [26, 27]

$$\begin{aligned} E_a^\Gamma &= 1,349 + 0,668x + 0,76x^2 \\ E_g^X &= 1,85 - 0,06x + 0,71x^2 \end{aligned}$$

Energy gap for direct gap composition ($0 < x \leq 0,63$) at 300 K:

$$E_g = 1,34 + 0,69x + 0,48x^2$$

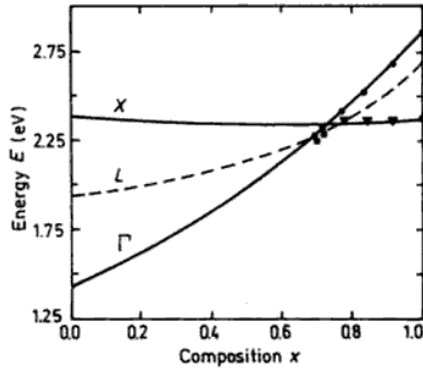


Fig.2: Material composition dependence of the Γ , L, and X-band gaps $\text{Ga}_x\text{In}_{1-x}\text{P}$ at 10 K[25].

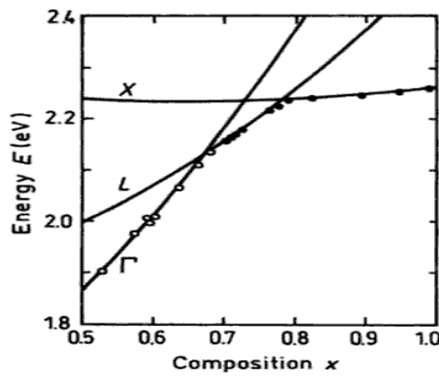


Fig.3: Material composition dependence of the Γ , L, and X-band gaps $\text{Ga}_x\text{In}_{1-x}\text{P}$ at 300 K[27].

For materials where the band gap changes between direct and indirect the relative electron mass of the lowest band is considered. Then a quadratic interpolation of the masses is used as a function of the material composition of an alloy $\text{Ga}_x\text{In}_{1-x}\text{P}$ [28-29]:

$$\begin{aligned} m_{\Gamma}^* &= 0.17 - 0.172x + 0.084x^2 \\ m_{\text{L}}^* &= 0,63 + 0.13x \\ m_{\text{X}}^* &= 0,667 + 0.13x \end{aligned}$$

For materials where the band gap changes between direct and indirect the relative electron mass of the lowest band is considered. Then a quadratic interpolation of the masses is used as a function of the material composition of an alloy $\text{Ga}_x\text{In}_{1-x}\text{P}$ [28-29]:

$$\begin{aligned} m_{\Gamma}^* &= 0.17 - 0.172x + 0.084x^2 \\ m_{\text{L}}^* &= 0,63 + 0.13x \\ m_{\text{X}}^* &= 0,667 + 0.13x \end{aligned}$$

For the case of InP, it is found that $m_{\Gamma} = 0.082$, and $m_{\text{X}} = 0.418$, while for the case of GaP, it is found that $m_{\Gamma} = 0.15$, and $m_{\text{X}} = 0.5$. The dielectric constant or relative permittivity ϵ_r is one of the basic properties of semiconductor. The permittivity's of alloy materials $\text{Ga}_x\text{In}_{1-x}\text{P}$

are interpolated from the values of the *basic materials* as a linear function of x [28]:

$$\begin{aligned} \epsilon_0 &= 1.29x + 11.11 \\ \epsilon_{\infty} &= 0.44x + 9.113 \end{aligned}$$

The values of the mass densities of the basic materials are well-known, and are used to model the values for alloy materials. A linear change between the values of basic materials is used [28]:

$$\rho = (0.652x + 4.14) \cdot 10^3$$

The lattice constant of a ternary alloy $\text{Ga}_x\text{In}_{1-x}\text{P}$ can be expressed as a linear combination of the lattice constants of the two forming binary alloys [28]:

$$a = 5.4505 - 0.4182x$$

3. Results

Fig. 3 shows the electron drift velocity versus the electric field simulated for the bulk InP. We note that initially the electron drift velocity monotonically increases with the applied electric field strength, reaching a maximum of about $2.5 \times 10^7 \text{ cm.s}^{-1}$ when the applied electric field strength is around 10 kV/cm.

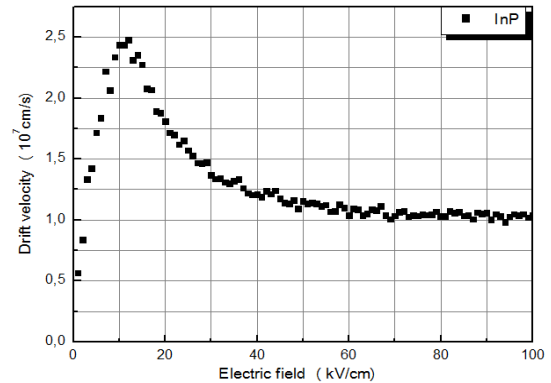


Fig. 3: The velocity-field characteristic associated with bulk InP.

For applied electric fields strengths in excess of $\approx 10 \text{ kV/cm}$, the electron drift velocity decreases in response to further increases in the applied electric field strength, i.e., a region of negative differential mobility is observed, the electron drift velocity eventually saturating at about $1 \times 10^7 \text{ cm.s}^{-1}$ for sufficiently high applied electric field strengths.

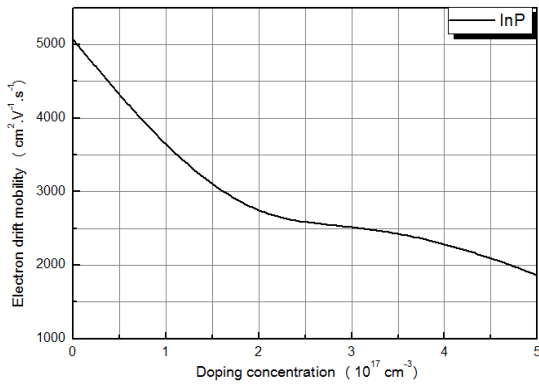


Fig. 4: Mobility of electrons as a function of the electric field in the InP

If we examine the average electron energy as a function of the applied electric field strength, shown in **Fig. 5**, we see that there is a sudden increase at around 6 kV/cm; this result was obtained from the same steady-state InP Monte Carlo simulation of electron transport as that used to determine **Fig. 5**.

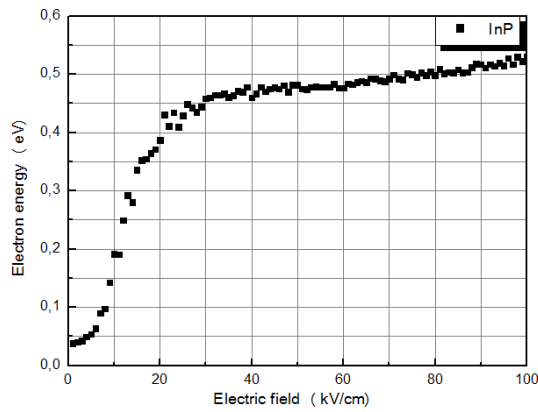


Fig.5: The average electron energy as a function of the applied electric field for bulk InP.

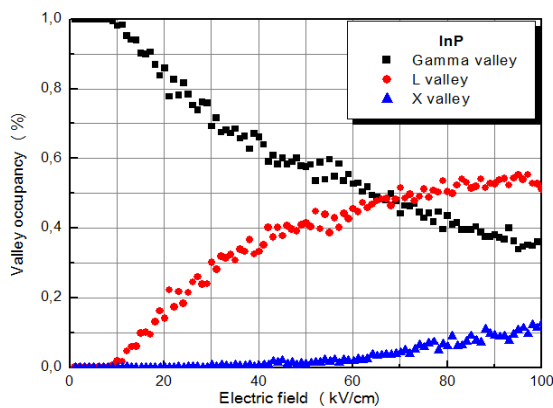


Fig.6: The valley occupancy as a function of the applied electric field for the case of bulk InP.

In order to understand why this increase occurs, we note that the dominant energy loss mechanism for many of the III-V compound semiconductors, including bulk InP, is polar optical phonon scattering. When the applied electric field strength is less than 6 kV/cm, all of the energy that the electrons gain from the applied electric field is lost through polar optical phonon scattering. The other scattering mechanisms, i.e., ionized impurity scattering, piezoelectric scattering, and acoustic deformation potential scattering, do not remove energy from the electron ensemble, i.e., they are elastic scattering mechanisms. Beyond certain critical applied electric field strength, however, the polar optical phonon scattering mechanism can no longer remove all of the energy gained from the applied electric field. Other scattering mechanisms must start to play a role if the electron ensemble is to remain in equilibrium. The average electron energy increases until inter-valley scattering begins and an energy balance is re-established.

In **Fig. 6**, we also plot the fractional electron occupancy of the central conduction band valley as a function of the applied field for zinc blend InP at 300 K, these results being from Monte Carlo simulations of electron transport in this material. We see that intervalley transitions, as indicated by a decrease in the occupancy of the central valley, do indeed begin in the neighborhood of 10 kV/cm. As the applied electric field is increased, the average electron energy increases until a substantial fraction of the electrons have acquired enough energy in order to transfer into the upper valleys. As the effective mass of the electrons in the upper valleys is greater than that in the lowest valley, the electrons in the upper valleys will be slower. As more electrons transfer to the upper valleys, the electron drift velocity decreases. This accounts for the negative differential mobility observed in the velocity-field characteristic depicted in **Fig. 4**.

In **Fig. 7**, the simulated electron drift velocity is plotted as function of applied electric field in Zinc blend GaP, these results being obtained from Monte Carlo simulations of electron transport at 300 K and electron concentration is equal to 10^{14} cm^{-3} . Gallium Phosphide “GaP” has an indirect band gap and at lower electric fields, so electrons occupied X satellite valley at first; so it is expected that its velocity-field curves does not have a peak. At higher electric field, inter-valley optical phonon emission dominates causing the drift velocity to saturate at around $0.8 \times 10^7 \text{ cm.s}^{-1}$.

In **Fig. 8**, we also plot the average energy of electrons in Zinc blend GaP as a function of the applied field. It is clearly see that energy curves demonstrate a higher monotonic increasing with increasing of external field at first. This increase in the average energy continues until the intervalley energy separation is achieved, at which point many of the electrons will have transferred from the central valley to the upper valleys.

The valley occupancies for the X, Γ and L valleys as a function of the applied field for Zinc blend GaP at 300 K are illustrated in Fig. 9. We see that intervalley transitions, as indicated by a decrease in the occupancy of the central valley X. As the applied electric field is increased, the average electron energy increases until a substantial fraction of the electrons have acquired enough energy in order to transfer into the upper valleys L and Γ . As the effective mass of the electrons in the upper valleys is greater than that in the lowest valley, the electrons in the upper valleys will be slower. As more electrons transfer to the upper valleys, the electron drift velocity decreases. The drift velocity is plotted in Fig. 10 function of applied electric field in InP and GaP with temperature as a parameter. For the calculations a fixed doping concentration of $1 \times 10^{17} \text{ cm}^{-3}$ was used. It is well known that temperature plays a decisive role in influencing the velocity-field characteristics of semiconductors occur. We note that the form of the velocity-field characteristic changes substantially as the temperature is increased. In particular, the peak drift velocity and the saturation drift velocity are found to decrease substantially with increased temperatures.

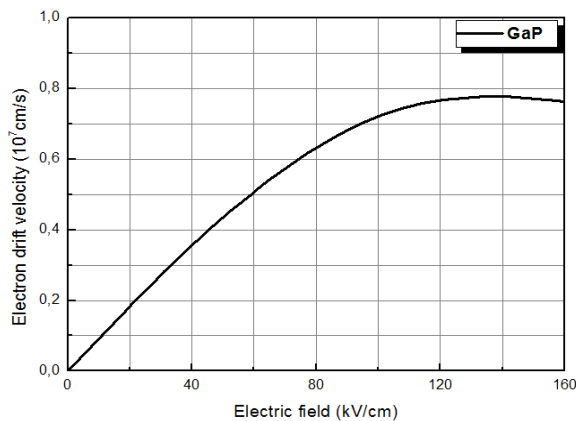


Fig. 7: The velocity-field characteristic associated with bulk GaP.

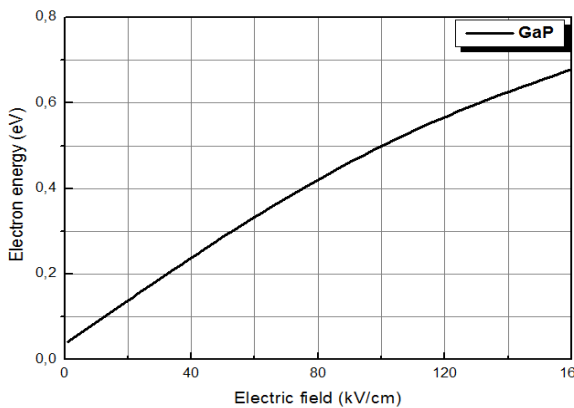


Fig.8: The average electron energy as a function of the applied electric field for bulk GaP

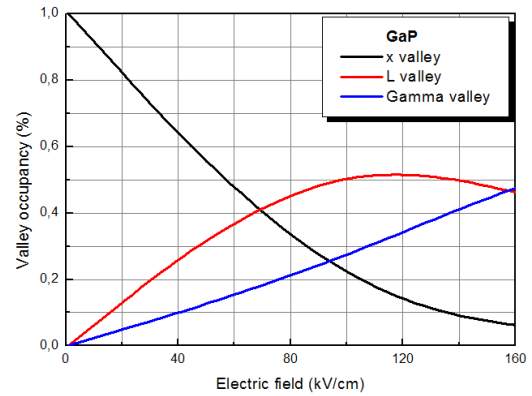


Fig.9: The valley occupancy as a function of the applied electric field for the case of bulk GaP.

It is interesting to note that the low field mobility increases as the temperature is lowered, whereas, the saturation velocity shows a less pronounced temperature dependence. This can be explained by noting that under low field conditions, scattering is dominated by acoustic phonons, ionized impurity, and polar optical phonon absorption which are all suppressed at lower temperatures leading to the improvement in mobility. At low fields for temperatures up to 300 K the hump in the velocity field characteristics is due to impurity scattering. At elevated temperatures the hump disappears due to the dominance of polar optical phonon scattering along with a drastic reduction in impurity scattering, the peak drift velocity decreases from about $2.76 \times 10^7 \text{ cm.s}^{-1}$ at 77 K to about $2.10 \times 10^7 \text{ cm.s}^{-1}$ at 500 K for InP and $0.9 \times 10^7 \text{ cm.s}^{-1}$ at 77 K to about $0.6 \times 10^7 \text{ cm.s}^{-1}$ at 500 K for GaP.

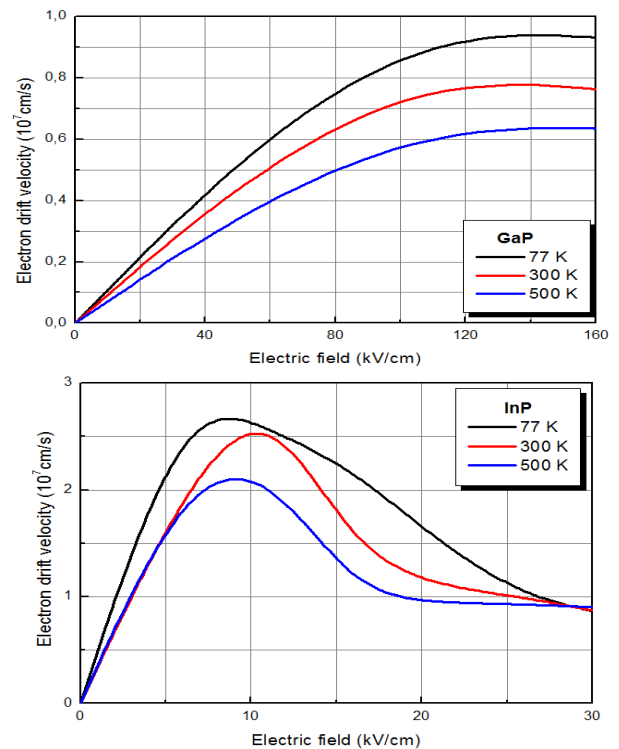


Fig. 10: Electron steady-state drift velocity in bulk InP and GaP as a function of applied electric field at various lattice

temperatures **Fig.11** shows the variation of the steady-state drift velocity as a function of the applied electric field for three different ionized impurity concentrations at room temperature for InP and GaP. The influence of doping becomes particularly noticeable for doping concentrations $1 \times 10^{18} \text{ cm}^{-3}$; the peak drift velocity decreasing markedly with further doping. the position of the peak velocity moves and decreases from about $2.5 \times 10^7 \text{ cm s}^{-1}$ at $1 \times 10^{14} \text{ cm}^{-3}$ to about $1.72 \times 10^7 \text{ cm s}^{-1}$ at $1 \times 10^{18} \text{ cm}^{-3}$ for InP and $0.76 \times 10^7 \text{ cm s}^{-1}$ at $1 \times 10^{14} \text{ cm}^{-3}$ to about $0.63 \times 10^7 \text{ cm s}^{-1}$ at $1 \times 10^{18} \text{ cm}^{-3}$ for GaP.

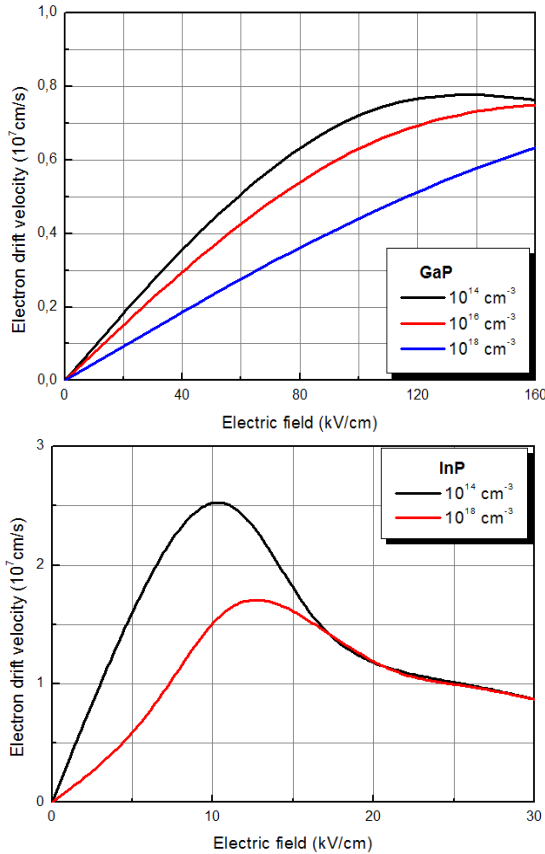


Fig. 11: Electron steady-state drift velocity in bulk InP and GaP as a function of applied electric field at various donor concentration.

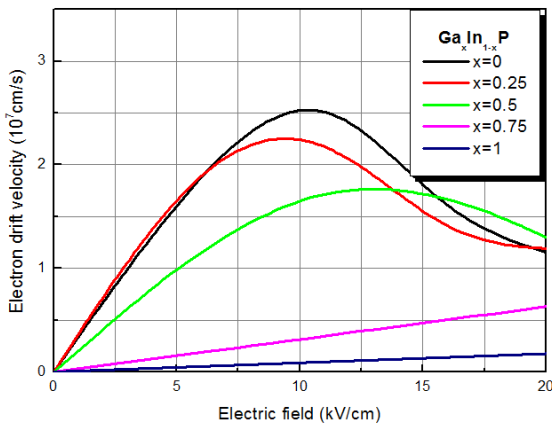


Fig. 12: The velocity-field characteristic associated with bulk GaIn_xP .

The steady-state electron velocity-field for GaIn_xP doped to 10^{18} cm^{-3} , at 300 K is presented in **Fig. 12**.

The dependence of the velocity-field relationship on increasing Ga mole fraction in GaIn_xP arises mainly from increases in the band-gap, the separation and the effective mass. The increasing electron effective mass, in the central valley, with increasing Ga mole fraction results in decreasing low field mobility. With increasing Ga mole fraction the valley separation increases with a consequent increase in the critical electric field, defined as the electric field where the velocity peaks. The increase in separation with increasing Ga mole fraction also results in a reduction in the intervalley scattering rate with a consequent decrease in the population in the upper valley and higher drift velocity at high fields. Especially under low fields, The steady-state electron velocity in $\text{AlGa}_{1-x}\text{As}$ is significantly degraded when x is increased to 0.3. Therefore, steady-state electron velocity in $\text{Ga}_{0.51}\text{In}_{0.49}\text{P}$ is higher than that of $\text{Al}_{0.3}\text{Ga}_{0.7}\text{As}$ under moderately high field strengths.

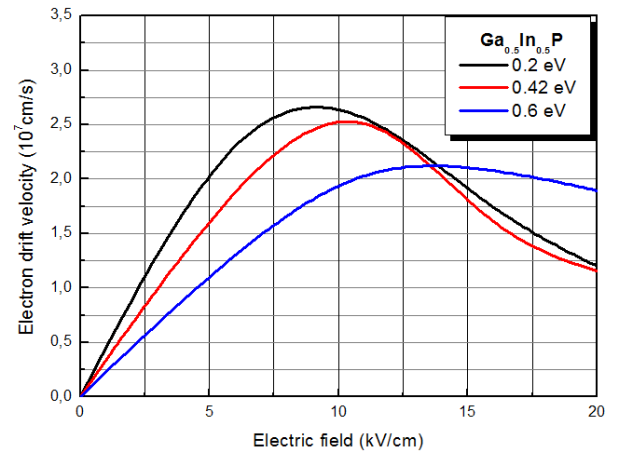


Fig. 13: Electron drift velocity versus electric field for different alloy scattering potentials in bulk GaIn_xP .

The effects of different values of ΔU on the transport of electrons in bulk GaIn_xP using the single particle Monte-Carlo program have been compared. The results of the transport simulations are shown in **Fig. 13**. The general trend in the velocity-field curves is a reduction of the drift velocity with increased alloy scattering potential. This is expected as an increase in alloy potential increases the total scattering rate and decreases the electron free flight time. so, if the alloy potential is increased, a larger field is needed to achieve a given level of L valley population. This can also be explained by the reduction of the time between collisions. As the free flight time falls the energy gained in this time decreases, and so a higher field is needed for the electron to attain the energy at which scattering to the L valleys becomes possible. A direct consequence of this is that the electron population in the Γ valley at any given field increases with alloy scattering strength and results in the shift of the peak velocity to higher fields seen in **Fig. 13**. If we compare the transport

results for GaP with those for GaIn_xP with $\Delta U = 0$ eV, we see the effect due to the changes in band structure and material parameters from alloying alone. As expected, the alloy has a greater low field mobility and higher peak velocity which is in turn because it has a lower Γ valley effective mass and a larger $\Delta E_{\Gamma L}$. The alloy also has a lower saturation velocity due to its larger satellite valley effective masses.

Conclusions:

In conclusion, we have presented low-field electron transport properties of GaIn_xP. Under moderately high field strengths, average electron velocity in GaIn_xP has been found to be higher than that of AlGa_xAs at the most widely used Al mole fraction of 0.3. In this paper we have introduced and examined the effects of alloy concentration of bulk GaIn_xP, and how this affects the transport properties, especially the average drift velocity, predicted by our Monte-Carlo simulation programs. We found that, for $x = 0.5$, the alloy scattering potential ΔU had an important effect on the carrier velocity, as ΔU increased the scattering rate increased and the carrier velocity was reduced. However, for the most of the range of ΔU considered and especially the value fitted to experimental results $\Delta U = 0.42$ we found a higher low field mobility and increased peak velocity over that for GaP, due to the smaller Γ valley effective mass and larger $\Delta E_{\Gamma L}$ in the alloy. We have found that (with $\Delta U = 0.42$) increasing Gallium concentration:

- Generally improved low field mobility, due to the smaller Γ valley effective mass,
- Increased the peak velocity, because of the larger value of $\Delta E_{\Gamma L}$,
- Reduced the saturation velocity, which we attributed to the larger satellite valley effective masses.

References

[1] Vedam Ramamurthy, AllaSrivani et G Veeraraghavaiah, "Investigation in Nano III-V ternary In_xGa_{1-x}P semiconductor materials by chemical vapor deposition", International Journal of Physical Research, 2 (2) (2014) 37-39.
 [2] Ariza C. H, Rev. Acad. Colomb. Cienc., 27 104, (2003), pp. 357-369.
 [3] S. Dissanayake, S. X. Huang, H. X. Jiang and J. Y. Lin, "Charge Storage and Persistent Photoconductivity in a CdS_{0.5}Se_{0.5} Semiconductor Alloy", Physical Review B, Vol. 44, No. 24, 1991, pp. 13343-13348. doi:10.1103/PhysRevB.44.13343.
 [4] S. Krishnamurthy, A. Sher, M. Madou and A.-B. Chen, "Semiconductor Alloys for Fast Thermal Sensors," Journal of Applied Physics, Vol. 64, No. 3, 1988, pp. 1530- 1532. doi:10.1063/1.341828.

[5] S. Strite and H. Morkoc, American Vacuum Society, B10 4, (1992), pp. 1237-1266.
 [6] Y.H. Wang and K.W. Lee, "Liquid Phase Oxidation on InGaP and its Applications", Adv. In solid state circuits technologies, ISBN 978-953, pp.446, (2010).
 [7] M.J. Mon and E. A. Fitzgerald, J. of Appl. Phys. 105 013107, (2009).
 [8] G.R.Moriarty, M.Kildemo, J.T.Beechinor, M.Murtagh, P.V.Kelly, G.M.Crean and S.W.Bland, "Optical and structural properties of InGaP heterostructures", Thin Solid Films, 364 244-248 (2000).
 [9] P.Emst, C.Geng, G.Hahn, F.Scholz, H.Schweizer, F.Philip, and A. Mascarehas, J.Appl. Phys. 79, 2633(1996).
 [10] Harrison J. W. and Hauser J. R. 1976 J. Appl. Phys. 47 292.
 [11] Harrison J. W. and Hauser J. R. 1976 Phys. Rev. B. 13 5347.
 [12] Asch A. E. and Hall G. L. 1963 Phys. Rev. 132 1047.
 [13] Littlejohn M. A., Hauser J. R., Glisson T. H., Ferry D. K., and Harrison J. W. 1978 Solid State Electron. 21 107.
 [14] M. A. Littlejohn et al., "Alloy scattering and high field transport in ternary and quaternary III-V semiconductors (FET model)," Solid-State Electron., vol. 21, pp. 107-114, Jan. 1978.
 [15] Marsh J. H., Houston P. A., and Robson P. N. 1981 Proceedings of the 17th International Symposium on Gallium Arsenide and Related Compounds, Vienna 1980 Institute of Physics, London. p621.
 [16] Basu P. K. and Nag B. R. 1983 Appl. Phys. Lett. 43 689.
 [17] V. W. L. Chin, B. Zhou, T. L. Tansley, and X. Li, "Alloy-scattering dependence of electron mobility in the ternary gallium, indium, and aluminum nitrides," J. Appl. Phys., vol. 77, pp. 6064-6066, 1995.
 [18] J. C. Phillips, "Ionicity of the chemical bond in crystals," Rev. Mod. Phys., vol. 42, pp. 317-354, 1970.
 [19] Schubert, E. Fred, Thomas Gessmann, and Jong Kyu Kim. Light emitting diodes. John Wiley & Sons, Inc., 2005.
 [20] Adachi S. 1982 J. Appl. Phys. 53 8775.
 [21] Adachi S. 1985 J. Appl. Phys. 58 R1.
 [22] Varshni Y P. Temperature dependence of the energy gap in semiconductors. Physica, 1967, 34(6): 149.
 [23] Pansh, M. B. and H. C. Casey Jr., J. App. Phys. 40, 1 (1969) 163-167.
 [24] t'Hooft, G. W. C. J. B. Riviere, M. P. C. Krijn, C. T. H. F. Liedenbaum, and A. Valster, Appl. Phys. Lett. 61, 26 (1992) 3169-3171.
 [25] Auvergne, D., Merle, and H. Mathieu, Solid State Commun. 21, 5 (1977) 437-439.
 [26] Lange, H., Donecker, and H. Friedrich, Phys. Stat. Solidi (b) 73, 2(1976) 633-639.
 [27] Krutogolov, Yu. K., S. v. Dovzhenko, S. a. Diordiev, L. I. Krutogolova, Yu. I. Kunakin, and S. A. Ryzhikh, Sov. Phys. Semicond. 23, 5 (557)-558.

[28] Dessemme, F., "Etude théorique et optimisation de transistors à effet de champ de la filière InP et de la filière GaN", Doctorat Thesis, USTL Lille, 1998.

[29] M. Levinshtein, S. Rumyantsev, "Handbook Series on Semiconductor Parameters", volume 2 ternary and

quaternary III-V Compounds, 1999 by world Scientific Publishing Co. Pte.Ltd.